Design and Investigation of PA Controller for Driving Nonlinear Electro Hydraulic Actuator with New Active Suspension System Model

Ali Al-Zughaibi, Yiqin Xue, Roger Grosvenor, Aniekan Okon

Abstract

Fully active electrohydraulic control of a ¼-car test rig is considered from both a modelling and experimental point of view. This paper develops a nonlinear active hydraulic design for the active suspension system, which improves the inherent trade-off between ride quality and suspension travel. The novelty is in the use of pole assessment (PA) controller to drive a nonlinear active suspension with a new insight into the model through consideration of a new term, friction forces. Therefore, this model has taken into account the dynamic inclination angle $(\alpha \mp \Delta\alpha)$ between linkage and actuator regardless of the designer made an only vertical motion (bounce mode) of the wheel and body units. The second contribution of this paper is investigated the control force generation, therefore, the nonlinear hydraulic actuator whose effective bandwidth depends on the magnitude of the suspension travel, which is incorporated the dynamic equation of servovalve, is deeply researched. The nonlinear friction model is accurately established, relies on the dynamics system analysis and the fact of slipping the body on lubricant supported bearings; this model will caption all the friction behaviours that have been observed experimentally. Additionally, the hydraulic system is used to generate the system inputs as a road simulator. The controller smoothly shifts its focus between the conflicting objectives of ride comfort and rattle space utilisation, softening the suspension when suspension travel is small and stiffening it as it approaches the travel limits. Thus, the nonlinear design allows the closed-loop system to behave differently in different operating regions. The improvement achieved with our design is illustrated through comparative experimental and simulations. C++ compiler environment is used to simulate

the physical system to be controlled. The results show good servo control and fast regulation of abrupt disturbances.

Keyword: New active suspension, friction force, nonlinear hydraulic actuator, dynamic servovalve, PA control.

NOTATION

A 5x5-System matrix	K_{fa} Servovalve flow constant
A/D Converter analog to digital	K_{ba} Forward gain
A_c Actuator cross-sectional area = 2.46e-4(m^2)	K_{sa} Linear servovalve flow constant
B 5x1-Input vector	L_d Free length of viscous damping = 0.342(m)
b_d Viscous damping = 260 (N/m. s^{-1})	M_b Body mass = 240 (kg)
b_t Tyre damping = 3886 (N/m. s^{-1})	M_c Controllability matrix
B_{va} Actuator viscous damping = 300 (N/m. s^{-1})	M_r Tyre mass = 5 (kg)
C 3x3-Output matrix	M_T Total mass = 285 (kg)
C_e Tracking parameter	M_w Wheel mass = 40 (kg)
D Viscous coefficient (N/m/s)	u_a Servovalve control
D/A Converter digital to analog	P_{1a},P_{2a} Pressures (N/ m^2)
ea Control signal	P_{sa} Supply pressure = 200e5 (N/ m^2)
e1 Curvature degree	Q1a, Q2a Flow rates (m^3/s)
F_{fric} Friction force (N)	R_{ia} Internal leakage resistance=2.45e11 (N/ m^5/s)
F_{hyd} Hydraulic force (N)	T Transformation matrix
x State vector	V Actuator chamber and hose volume= 7.13e-5 (m^3)
x_{sa} Spool movement (m)	V_2 Dynamic actuator volume side 2 (m^3)
g Gravitational constant (m/s^2)	V_1 Dynamic actuator volume side 1 (m^3)
G D/A convertor gain	β_e Effective bulk modulus =1.42e9 (N/ m^2)
G_d 5x1-Disturbance vector	ξ damping ratio
k_t Tyre stiffness = 9.2e5 (N/m)	ω_d Damped natural frequency (rad/s)
k_a Servovalve gain	ω_n Undamped Natural frequency (rad/s)
k_s Spring stiffness = 2.89e4 (N/m)	μ Friction coefficient
K 1x5-State feedback gain vector	τ_a Time servovalve constant (s)
K_1 1 x 5-State feedback gain vector for the controller	θ the construction angle of passive units= 45 °
K_2 5 x 5-Transducer gain matrix	α Inclined hydraulic actuator angle = 27 °

Al-Zughaibi Ali was a lecturer at the Engineering College, University of Kerbala, Iraq. He is currently a PhD student at the School of Engineering, Cardiff University, Cardiff, UK, (Email: alialzughaibi2016@gmail.com).

Xue Yiqin is with the Cardiff School of Engineering, Cardiff University, Cardiff, UK, (Email: Xue@cardiff.ac.uk)

Grosvenor Roger is with the Cardiff School of Engineering, Cardiff University, Cardiff, UK, (Email: Grosvenor@cardiff.ac.uk)

Aniekan Okon is with the Cardiff School of Engineering, Cardiff University, Cardiff, UK, (Email: okonaa@cardiff.ac.uk)

1. Introduction

Vehicle suspensions have remained a hot research topic due to their essential role in ride comfort, vehicle safety, road damage minimisation and the overall vehicle performance. Passive suspension (PS), which has been modelled and discussed in detail by same authors as reported in (1), is possibly the most commonly used and is found in most vehicles. However, in the real world, the passive suspension has no means of adding external energy to a system because it contains only passive elements, such as a damper and spring. By contrast, active suspension (AS) can supply power from an external source and generate force to achieve the optimal desired performance, as is organised explicitly within the available test rig. From this point of view, AS with regard to pole assignment (PA) control is investigated in this study. A critical question that emerges in the outline of state variable compensators is whether every pole of the closed-loop system can be discretionarily placed in the complex plane. The poles of the closed-loop system are equivalent to the eigenvalues of the system matrix in state variable configuration. If the system is controllable, then it can benefit the planned goal of setting the poles precisely at desired locations to meet performance specifications. Full-state feedback design commonly relies on pole-placement techniques can be found into (2).

A further vital synthesis question examines whether, given a model, one could efficiently synthesise a controller such that the closed-loop poles are in predefined areas. This paper will demonstrate this to ascertain that it is conceivable. The PA was an essential concept

in control synthesis as reported by (3). The closed-loop systems, obtained by using either state feedback or output feedback, are described by four new system matrices (A, B, C, and D). The purpose of adding feedback is to improve the system attributes to some degree. The impact of feedback on the properties of controllability, observability, and stability need to be accurately understood as mentioned by (4).

Yang et al. (5) focused their study on using the state-space representative for a wheel organised drive structure arranged with both vehicle body height changing dimensions and wheel driving limit. They designed a proportional-integral-derivative (PID) controller to examine the closed-loop system stability within time-varying sampling.

Additionally, to improve the stability and ride handling the performance of the vehicle, AS systems have attracted a significant amount of research interest in the past few decades and comprehensive surveys on related research are found in publications. These have included classical PID control (6), multi-objective control (7), a robust design method of adaptive sliding mode control was derived (8), active force control based architecture in characterising the twin rotor MIMO system (9). Also, distributed control literature provides numerous beneficial approaches for achieving stability. It was shown by (10) that stability of a formation depends on the agent model and eigenvalues of the graph Laplacian. This fact was later used by (11) to derive a state-feedback controller, which works for any graph topology, only the gain of the controller needs to be adjusted. A controller design presented by (12) uses an LQR-like approach to achieve stability. Adaptive strategies can also be used (13), (14).

Herman and Sebek (15) researched to design state feedback based on a single-agent model by using a sufficiently large coupling gain and meeting specific criteria, the control law was not only stabilising but also linear quadratic (LQ) optimal. Such control law was then applied to controller design for asymmetric vehicular platoons.

Recently, Xinbo Ma et al. (16), proposed a multi-objective control strategy that probably provided effective damping force adjustment and improved the vertical dynamic performance of vehicles comprehensively. Moreover, the hardware-in-the-loop test can offered a guidance for the practical application of the damping force control in real vehicles. Although this acritical mentioned a good information about damper adjustment but, with ignoring how to generate the control force.

A three-layer hierarchical strategy presented by (17), for integrated control of the active suspension system, active front steering system and direct yaw moment control system pointing to improve the lateral and vertical performance of the vehicle.

Jing Zhao et al. (18) focused their study on wheelbase preview (WP) control. Currently, the WP overlooks the road excitation within the wheelbase. Therefore, when the vehicle is cornering, the tyre is bumping off, or the tyre is suffering from air leakage, the previewed information from the front wheel could be affected, resulting in a mistaken road prediction to the rear wheel.

From another perspective, an interesting problem dealing with the issue of friction and lubrication in sliding bearings should be considered. This problem is very challenging and has been the subject of several studies, such as the applications covered water-lubricated shipboard bearings (19), (20), (21); and (22). These studies were dominated by experimental tests of section models that emulated the actual bearing dynamics. Different dynamic characteristics were predicted from the numerical simulation of the equations of motion and were exhibited by a bifurcation diagram revealing different regimes. These regimes include modulated response signals characterised by two frequency responses, an intermittent on-off movement representing the incipient of squeal behaviour, and limit cycles accompanied by high-frequency components. The occurrence of each regime mainly depends on the value of the slope of the friction-speed curve.

The role of nonlinearity due to the friction-speed curve as well as the time variation of the friction coefficient has been considered in many other studies. The time variation of the static friction in relation to stick-slip vibration has been studied experimentally (23), (24), (25), (26); and (27). These studies revealed two factors responsible for increasing the value of the static friction coefficient, with time. These are the creep rate of compression of the asperities, increasing in the junction areas, and the shear strength of the junctions due to the existence of the cold-welding effect. Experimental characterisation of interfacial forces in metal-to-metal contact under harmonic excitation revealed that both the static and the kinetic friction coefficients exhibit random time variations (27).

Pilipchuk et al. (28) deliberated the brake squeal phenomenon was observed at the last phase of braking process causes the decelerating sliding, which was very slow as compared to the temporal scales of friction-induced vibrations related with elastic modes of braking systems. A state and maximum friction coefficient estimation using the joint unscented Kalman filter presented by (29), and they considered a highly nonlinear vehicle model representing longitudinal and lateral dynamics.

Suspension system modelling and associated control design with influence vehicle response, therefore, this study, in contrast to all previous research studies, will be a unique to consider the body friction effects within the active quarter-car model system, accordingly, taking into account the actual orientation of the suspension units and test rig constriction. A new active suspension system model with the implementation of the nonlinear bearings body lubricant friction forces, in addition to systematic friction occurs inside the actuator, is considered. A hydraulic actuator is used instead of the spring and viscous damper units of the PS, to generate the hydraulic control force, as shown in Fig 1.

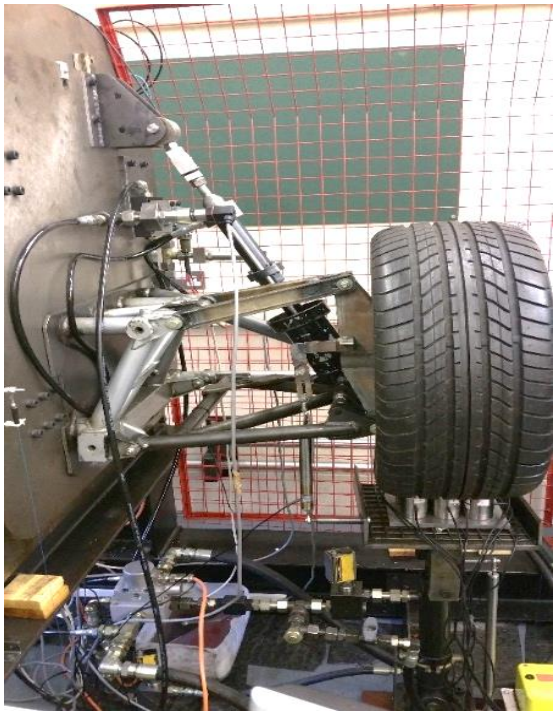

(a)

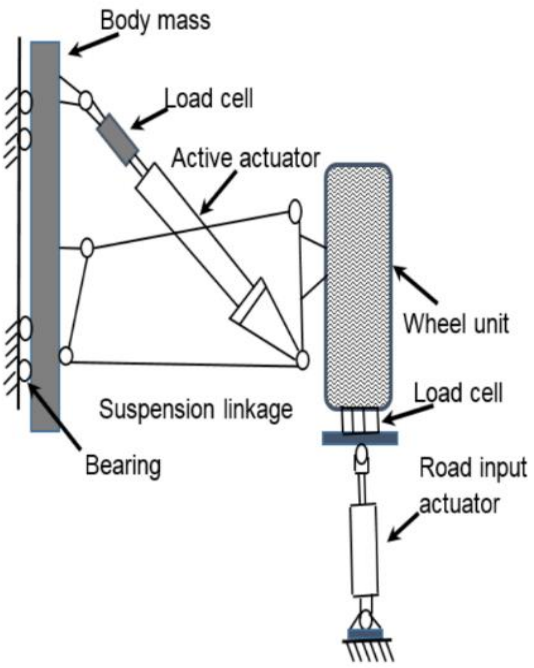

(b)

Fig. 1 a. Photograph of the active test rig b. Schematic diagram of test rig

Therefore, a nonlinear hydraulic actuator model covered by the dynamic of servovalve is investigated. The controller has been demonstrated in considerable much detail by using the state-space system. This work focuses on designing and investigating the PA controller to drive the nonlinear hydraulic active actuator in the AS and to ensure be achieved their target.

This study will test validity in two stages: the primary stage were carried out on the test rig platform to assess the behaviour of the PS real system. While, the second stage were performed on the C++ compiler and by using MATLAB Control System Toolboxes, a simulated model where it was easy to evaluate the performance with a mathematical approach. Therefore, a study has been made to develop an active suspension model for

improvement of the performance of a vehicle response through an implementation of the PA controller.

2. Road simulator

System input, road simulator input, is one of the essential aspects of experimental work or simulation; therefore, types of road excitation significantly affect the system responses and should be similar as possible to reality. There are two types of input system used in this study as follows:

2.1 Step road profile

In experiential work, the input used is mixed between the ramp and step with a definite amplitude value; this is with a drawback, which was a quite sharp and might be damaged the test rig. Therefore, a digital first order filter has been used through the C++ compiler within the PS stage. A proportional- integral (PI) control has been developed to ensure the input is sufficient for the requirement, as a results, which successfully achieved its target, the complete detail of the road input simulator for step input is demonestrated by (1). Accordingly, in addition to this input, it is of benefit to consider random profile inputs to show the controller's achievement and robustness.

2.2 Random road profile

Road surface roughness approximation has been commonly approximated through the use of the ISO 8608 classifications (30), (31), which are ranges of proposed PSD for different levels of roughness. Tyan et al. (32) established a one-dimensional sinusoidal approximation method based on these PSD specifications for use with quarter and half-vehicle suspension models. The ISO 8608 standard (33) proposes an approximated formula to obtain the PSD function of the road roughness as follows:

$$\Phi(\Omega) = \Phi(\Omega_o)(\frac{\Omega}{\Omega_o})^{-\omega} \quad [1]$$

Where, $\Omega = \frac{2\pi}{l}$ (rad/m) signifies the angular spatial frequency, l is the wavelength, and ω is the waviness, for most road surface $\omega = 2$. $\Phi_o \cong \Phi(\Omega_o)$, $\Phi(\Omega_o)$ is the reference PSD value for a given road type at the reference angular spatial frequency $\Omega_o = 1$ (rad/m). The reference values of the PSD at $\Omega_o = 1$ (rad/m) for different road modules are given by ISO 8608 (33), as shown in Table I. At low spatial frequency Equation [1] tends to infinity, so it was adopted by (32) to designate pavement roughness PSD as follows:

$$\Phi(\Omega) = \begin{cases} \Phi(\Omega_o)\Omega_1^{-2} & \text{for } 0 \le \Omega \le \Omega_1 \\ \Phi(\Omega_o)(\frac{\Omega}{\Omega_o})^{-2} & \text{for } \Omega_1 \le \Omega \le \Omega_N \\ 0 & \Omega_N \le \Omega \end{cases} \quad [2]$$

Table I: Road roughness values (29)

	Degree of roughness $\Phi(\Omega_o)$ $(10^{-6}m^3)$ for $\Omega_o = 1$ (rad/m)		
Road class	Lower limit	Geometric mean	Upper limit
A (very good)	-	1	2
B (good)	2	4	8
C (average)	8	16	32
D (poor)	32	64	128
E (very poor)	128	256	512

The values of Ω_1 and Ω_N has been suggested by the ISO 8606 standard to be 0.02π and 6π (rad/m) respectively (32), which covers a wavelength band of 0.333-100 m. In the current study, it was decided to use (34) analysis to modify (32). When the vehicle is travelling over a specified road segment of length l and constant velocity v, then the random road profile as a function of a travelled path s can be approximated using a superposition of $N(\rightarrow \infty)$ sine waves as reported by (34), as follows :

$$X_r(s) = \sum_{n=1}^{N} A_n \sin(\Omega_n s - \varphi_n) \quad [3]$$

Where the amplitude A_n is given by:

$$A_n = \sqrt{\Phi(\Omega_n)\frac{\Delta\Omega}{\pi}} \quad [4]$$

Where, $\Delta\Omega = \frac{\Omega_N - \Omega_1}{N-1}$ and $\varphi_n$is a random phase angle between (0, 2 π). The term Ω s in Equation [3] is equivalent to:

$$\Omega s = \frac{2\pi}{\lambda}s = \frac{2\pi}{\lambda}vt = \omega t \quad [5]$$

In which λ is the wavelength and ω (rad/s) is the angular frequency in the time domain. From Equations [3] and [4], the road profile in the time domain is given as follows:

$$X_r(t) = \sum_{n=1}^{N} A_n \sin(n\omega_0 t - \varphi_n) \quad [6]$$

Where, $\omega_0 = v\Delta\Omega$ (rad/s) is the fundamental temporal frequency in the time domain. Because the random road contains most of the human frequency sensitivity range and most of the road profiles are random, a random road profile is selected in the optimisation process with a very poor road roughness and a vehicle velocity of $v = 100$ km/h.

3. Passive suspension system

The dynamic equation of motion for the mass body test rig with the consideration of the friction forces for PS system, as previously researched by (1), is:

$$M_b.\ddot{X}_b = [k_s(X_w - X_b) + b_d(\dot{X}_w - \dot{X}_b)] - F_{fric} \quad [7]$$

Whereas, the dynamic equation of motion for the wheel is:

$$M_w.\ddot{X}_w = -[k_s(X_w - X_b) + b_d(\dot{X}_w - \dot{X}_b)] + k_t(X_r - X_w) + b_t(\dot{X}_r - \dot{X}_w) \quad [8]$$

Where, $\ddot{X}_b, \ddot{X}_w$ are the body and wheel acceleration (m/s^2) respectively.

4. Nonlinear friction forces model

Based on the observations and the dynamic system analysis, a stimulate friction model is developed. This model includes a stiction effect, viscous friction, Coulomb friction, and Stribeck effect. During acceleration, the magnitude of the frictional force at just after zero speed decreases due to Stribeck effects that mean the influence of the friction transfers from direct contact between the bearings and the body into mixed lubrication mode at low velocity; this possibly due to lubricant film behaviours.

This model has been able to give a more satisfactory explanation for the observation of removing the body dynamics fluctuation as was investigated by (1). In addition, the model simulates the symmetric hysteresis loops observed at the body bearings undergoing forcing inputs. In general, this friction model considers the static, stiction region, and dynamic friction, which consists of Stribeck effect, Coulomb friction and viscous friction.

4.1 Mathematical description of general friction model for AS

Because the friction has occurred at linear supported body bearings, it will, therefore, be supposed that the friction had the same behaviours as mentioned for PS (1). However, the friction presents some differences features depending on the types of input force and the quantity of vertical force according to replacement the active hydraulic actuator instead of the spring and viscous damper (PS units). The mathematical expression for the general friction model is consisting of three different sectors depending on the acceleration or deceleration and direction of the body velocity, as follows:

$$F_{fric} = \begin{cases} F_{hyd}\cos(\alpha \mp \Delta\alpha) - B_v(\dot{X}_b - \dot{X}_w) & \dot{X}_b = 0.0 \\ C_e e^{(|\dot{X}_b|/e1)} + \left[\frac{\mu M_w \ddot{X}_w}{\tan(\alpha \mp \Delta\alpha)}\right] + D\dot{X}_b & \dot{X}_b > 0.0 \\ -C_e e^{(|\dot{X}_b|/e1)} + \left[\frac{\mu M_w \ddot{X}_w}{\tan(\alpha \mp \Delta\alpha)}\right] + D\dot{X}_b & \dot{X}_b < 0.0 \end{cases} \quad [9]$$

Where, F_{fric}, is the total friction force in (N).

4.2 Mathematical of simple friction model

Equation (9) gives a general form for the friction, this model could be studied from the different point of view, it can be returned to two dominants parameters, the body velocity and the normal body force. The friction relative to the body velocity is named as damping friction, while Coulomb friction qualifies to the normal body force.

For simplicity, although the frictions model Equation [9], covered most of the observation friction phenomena, still it could be used a simple form through ignoring Coulomb friction. Therefore, the simple friction expression without Coulomb is:

$$F_{fric} = \begin{cases} F_{hyd}\cos(\alpha \mp \Delta\alpha) - B_v(\dot{X}_b - \dot{X}_w) & \dot{X}_b = 0.0 \\ C_e e^{(|\dot{X}_b|/e1)} + D\dot{X}_b & \dot{X}_b > 0.0 \\ -C_e e^{(|\dot{X}_b|/e1)} + D\dot{X}_b & \dot{X}_b < 0.0 \end{cases} \quad [10]$$

Equation [10] potentially demonstrates the simple friction model, which has been had the same three various sectors. The interesting point, implementing of this simple friction forms within the mathematical simulation model, also acquired an excellent agreement comparing with the experimental results regarding system response parameters. The urgent question is which one is more suitable for current case? Accordingly, as pervious investigation for PS system; the general friction model has been given more details to show their ability to highlight the hysteresis phenomena that should take place with this system input types as shown in Fig. 2.

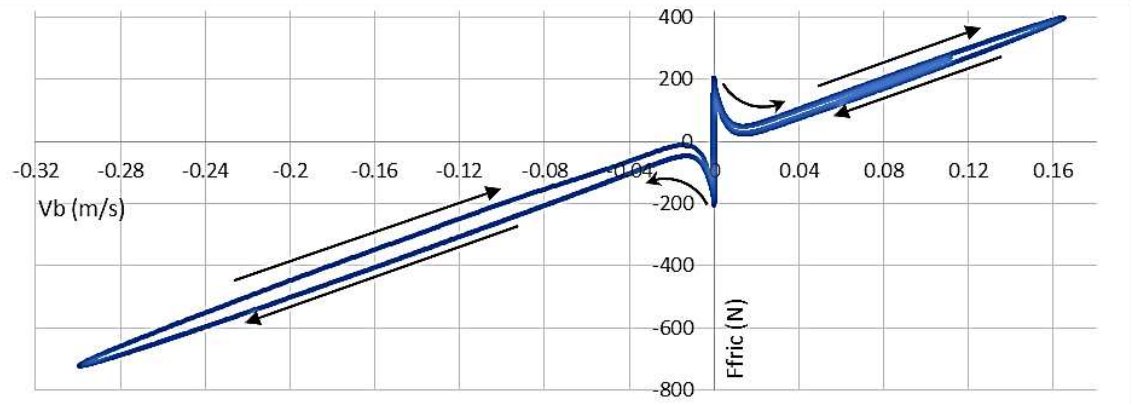

Fig. 2 General friction as function of the body velocity (Vb=$\dot{X}_b$) [1].

Whereas the simple friction has lost to display hysteresis as be demonstrated in Fig. 3. The comparison between the damping and Coulomb frictions is shown in Fig. 4.

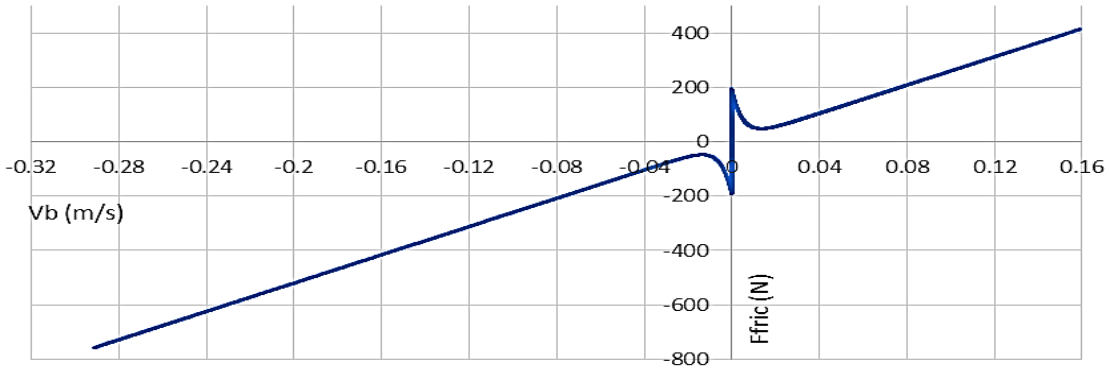

Fig. 3 Damping friction (without Coulomb friction), as function of the body velocity.

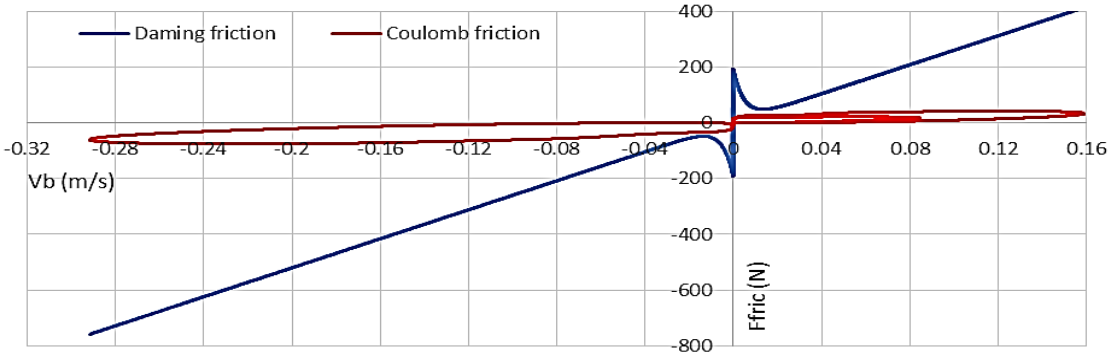

Fig. 4 Comparing between damping friction and Coulomb friction as function of the body velocity.

Figure 2 demonstrates the total nonlinear friction as a function of the body velocity for PS system. The test rig construction and the system input, which is with a history travels, are helping together to generate the hysteresis friction behaviours. This is depending on whether the body velocity is accelerating or decelerating, the velocity values are started from zero and just after velocity reversals, reaching the highest, and it was rebounded to zero or close to zero at steady state. Therefore, from Fig. 2, it is evidently seen that at $\dot{X}_b = 0.0$, the friction values are equal to the static friction, then it just crosses $\dot{X}_b = 0.0$, the friction directly dips relative to Stribeck affects, this could be because of the hydraulic layer behaviours. After that $\dot{X}_b >> 0.0$ helps the friction to be drawn the two hysteresis loops in a positive direction while when $\dot{X}_b < 0.0$, actions to generate a hysteresis loop in the opposite direction with a twice value regard to input force. Whereas, Fig. 3 shows the sample friction without Coulomb friction and the comparison between the damping and Coulomb friction is shown in Fig. 4.

A mathematical analysis, residual mean square (RMS), is used to find which one is accurate. Relatively, it is used two measured parameters X_b and $X_w - X_b$ to show the accuracy of considering the general or simple friction form. The RMS is accounted for the measured and mathematical simulation model results with and without Coulomb friction for the relative movements between the wheel and body, as follows:

$$(\mathrm{RMS})c = \sqrt{\frac{1}{N} * \sum((X_w - X_b)_m - (X_w - X_b)_{Sc})^2} \quad [11]$$

And,

$$(\mathrm{RMS}) = \sqrt{\frac{1}{N} * \sum((X_w - X_b)_m - (X_w - X_b)_S)^2} \quad [12]$$

Where, $(\mathrm{RMS})c$ and (RMS) are the RMS between measured and simulation values with and without considering Coulomb friction respectively, $(X_w - X_b)_m$ is the measured relative displacement. $(X_w - X_b)_{Sc}$ and $(X_w - X_b)_S$ are the simulation data with and

without implementing Coulomb friction, N is the total number of sample. Table II has demonstrated the RMS results.

Table II RMS results

Signal	(RMS)c	(RMS)
$(X_w - X_b)$	0.006362	0.006366
X_b	0.096267	0.096386

5. Hydraulic nonlinear system modelling

Electro-hydraulic servo systems (EHSS) are widely used in many industrial applications and mobile systems because of their high power-to-weight ratio, high stiffness, fast response, self-cooling, unique positioning capabilities, etc. However, the dynamical models of the EHSS have many uncertainties, which are consequences of physical characteristics, disturbances and load variations (35). The dynamic behaviour of these systems is highly nonlinear due to phenomena such as pressure-flow characteristics, hysteresis in flow gain characteristics, oil leakage, oil temperature variations, characteristics of valves near null, and so on. In practice, determining the exact dynamic model that will contain all the physical phenomena of EHSS presents a difficult task. The dynamics of hydraulic systems are highly nonlinear (36). A nonlinear, backstepping control technique in light of a high gain observer design was displayed for a single-rod electro-hydraulic actuator with a proportional model change and utilised for load pressure to establish the connection between displacement command and virtual command of load weight researched by (37). Fu et al. (38) mentioned the building up of the mathematical servovalve model, which the establishment of design and control were added to investigate its characteristic and influence factors in-depth. Maneetham et al. (39) presented a proportional derivative controller for high-speed nonlinear hydraulic servo system. Alleyne and Hedrick (40) considered the nonlinear dynamics of an electro-

hydraulic actuator in a quarter car active suspension model and used these dynamics to formulate a nonlinear control law.

However, in practice, the hydraulic dynamics significantly influence system responses as shown later. Therefore, the hydraulic modelling is investigated in the next section.

5.1 Servovalve nonlinear model

The piston is assumed to be supporting a vertical load acting such that it always attempts to retract the piston, that is, it still moves in the same direction. For open-loop control systems, a critically lapped servovalve spool is assumed, and for closed-loop control systems, asymmetrically underlapped servovalve spool is always considered.

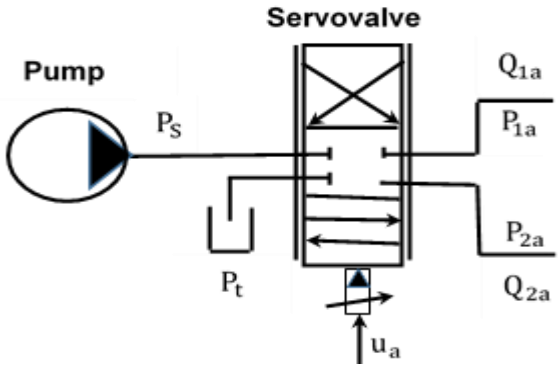

Fig. 5 Servovalve schematic diagram

Considering Fig. 5 and Fig. 1b, the servovalve schematic diagram and the schematic diagram for active system test rig respectively, and the conventional modelling (40) and (41). The servovalve equations are nonlinear equations whose flow rate outputs are functions of two inputs, voltage signal and a square root of pressure drop across the valve. Therefore, the flow rate relationships for both side are given by:

$$Q_{1a} = f(u_a, P_{1a}) \quad [13]$$

$$Q_{2a} = f(u_a, P_{2a}) \quad [14]$$

By considering a first-order servo system given by:

$$\dot{x}_{sa} = \frac{1}{\tau_a}(k_a u_a - x_{sa}) \quad [15]$$

Where τ_a (s) is time servovalve constant, k_a is gain of the servovalve, u_a (mv) is applied voltage, x_{sa} (m) is the servovalve spool movement and $\dot{x}_{sa}$ (m/s) is spool velocity.

Accordingly, depending on the direction of spool movement, the flow rate equation was developed into two cases (extending and retracting) with assuming that tank return pressure is negligible.

As a result the simplified servovalve equations for both cases are:

$$Q_{1a} = K_{fa}\, x_{sa}\sqrt{P_{sa} - P_{1a}} \quad [16]$$

$$Q_{2a} = K_{fa}\, x_{sa}\sqrt{P_{2a}} \quad [17]$$

5.2 Nonlinear actuator model and hydraulic force

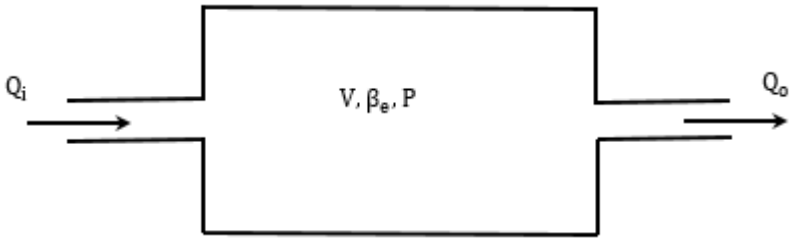

Fig. 6 Flows entering and leaving a control volume.

Considering a fluid control volume having input and output flow rates as shown in Fig. 6. A flow rate continuity equation is given in the form:

$$Q_i - Q_0 = \dot{V} + \frac{V}{\beta_{ea}}\dot{P} \quad [18]$$

Where, $\dot{V} = A_c(\dot{X}_b - \dot{X}_w)$

For mathematical analysis and regular control condition, approximately the mid-position of the actuator and the zero voltage signal of the servovalve, i.e. the operating condition, then extending and retracting can be defined by the positive and negative voltage signals or up and down spool movements.

If Q_{1a} and Q_{2a} signs are controlled by the spool valve direction, simplified actuator equations for both cases are:

$$Q_{1a} = A_c\left(\dot{X}_b - \dot{X}_w\right) + \frac{V}{\beta_{ea}}\dot{P}_{1a} \quad [19]$$

$$Q_{2a} = A_c\left(\dot{X}_b - \dot{X}_w\right) - \frac{V}{\beta_{ea}}\dot{P}_{2a} \quad [20]$$

Depending on the servovalve characteristic supplied by the manufacturer, no significant spool underlap, or overlap exists. Although often ignored, there are two sources of internal leakage: First, flow through the hydraulic amplifier, which is relatively constant; and second, flow around the spool, which varies with its position (42). The position-tracking problem of an EHSS with internal leakage in servovalve was investigated using the fuzzy logic approach in the controller design (43). Maximum internal leakage occurs at null; therefore, the internal leakages are ignored in this study. However, it was assumed that the hydraulic leakage characteristic is dominated by the actuator piston radial clearance effect, and the leakage effects must be included in the actuator equations. The net effects of cross-port leakage are to increase the damping characteristic of the actuator as the degree of leakage increases (44).

The oil leakage is a function of the pressure difference across both sides of the actuator and cross-port leakage resistance. Accordingly, the active system actuator flow rate equations include compressibility and cross-line leakage effects for both teams, could be written as:

$$\frac{V}{\beta_{ea}}\dot{P}_{1a} = Q_{1a} - A_c(\dot{X}_b - \dot{X}_w) - \frac{(P_{1a}-P_{2a})}{R_{ia}} \quad [21]$$

$$\frac{V}{\beta_{ea}}\dot{P}_{2a} = A_c(\dot{X}_b - \dot{X}_w) + \frac{(P_{1a}-P_{2a})}{R_{ia}} - Q_{2a} \quad [22]$$

The actuator hydraulic force is given by:

$$F_{hyd} = A_c(P_{1a} - P_{2a}) \quad [23]$$

6. Active suspension model

The free body diagrams of the car body and wheel unit is shown in Fig. 7, the model of the actively suspended ¼-car by implementing the new term, friction force, relative to test rig construction and the real dynamic position, by defining the actual dynamic orientation between the actuator and linkage, angle ($\propto \mp\Delta\propto$).

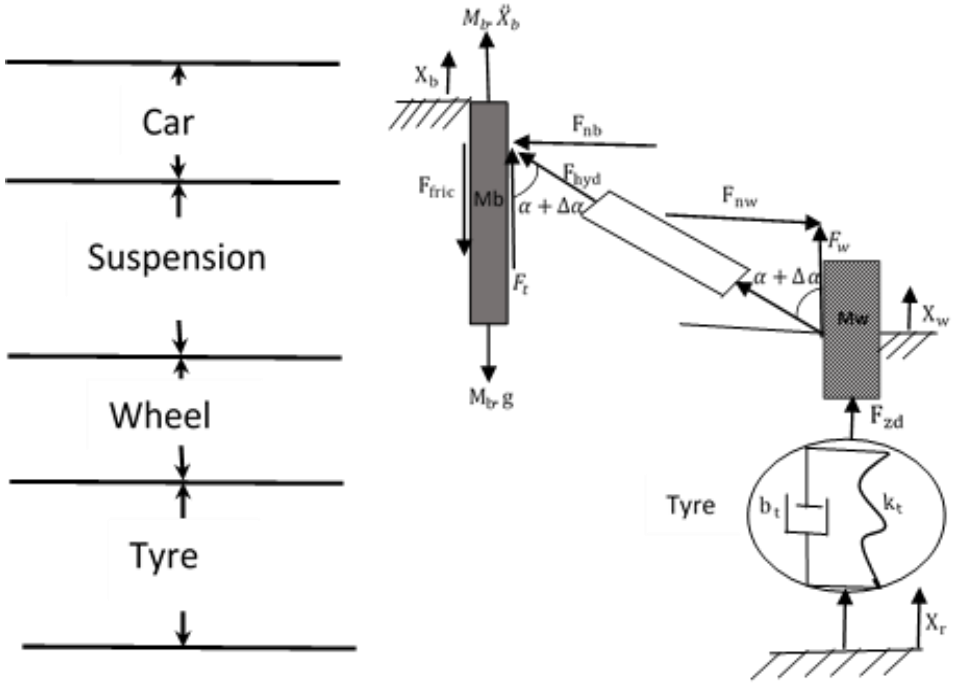

Fig. 7 Free body diagram of a quarter car and active suspension model.

The friction forces is the first time to be considered with the equation of motion in addition to the systematic friction that already has been occurred inside the actuator (viscous and Coulomb friction). In fact, the ¼-car research test rig mostly used to investigate and study the dynamic modelling and control of vehicle active suspension system, most of the previous researches were ignored the friction effects on the body that could be results insufficient information about system model and control. Therefore, revise the model by considering an accurate form surly contribute to identify a precise control and bush the knowledge in this field, from this point of views, the important of this contribution came.

The new equation of the body motion, by considering the bearings body friction in addition to the viscous friction, which occurs inside the hydraulic actuator, and wheel equations are:

$$M_b.\ddot{X}_b = [F_{hyd} - B_{va}(\dot{X}_b - \dot{X}_w)]\cos(\alpha \mp \Delta\alpha) - F_{fric} \quad [24]$$

$$M_w.\ddot{X}_w = -\left[F_{hyd}\cos(\alpha \mp \Delta\alpha) - B_{va}\left(\dot{X}_b - \dot{X}_w\right)\right] + k_t(X_r - X_w) + b_t(\dot{X}_r - \dot{X}_w) \quad [25]$$

In the case of small disturbances, linearised models of the power system around an equilibrium point are adequate for stability analysis and control design.

Therefore, it could be sufficient to use the characteristic linear servovalve equations as:

$$Q_{1a} = Q_{2a} = k_{sa}x_{sa} \quad [26]$$

Where

$$k_{sa} = k_{fa}\sqrt{P_{sa} - P_{1ass}} = k_{fa}\sqrt{P_{2ass}} = k_{fa}\sqrt{P_{sa}/2} \quad [27]$$

x_{sass}, is steady state servovalve spool movement relative to applied voltage and P_{1ass}, P_{2ass} are the steady-state pressures. At the null condition, $u_{ass} = 0$ ($x_{sass} = 0$), and $P_{sa}/2 = P_{1ass} = P_{2ass}$, for a critically lapped spool.

From Equations [21, 22, 23 and 27], it was found:

$$2k_{sa}A_c x_{sa} = 2A_c^2(\dot{X}_b - \dot{X}_w) + \frac{V}{\beta_{ea}}\dot{F}_{hyd} + \frac{2}{R_{ia}}F_{hyd} \quad [28]$$

Considering Equation [15], therefore, Equation [28] became,

$$2k_{sa}A_c u_a = 2A_c^2(\dot{X}_b - \dot{X}_w) + \frac{V}{\beta_{ea}}\dot{F}_{hyd} + \frac{2}{R_{ia}}F_{hyd} \quad [29]$$

The quarter-car response variables that need to be examined are:

1. Car body acceleration $\ddot{X}_b$
2. Suspension displacement $X_w - X_b$
3. Tyre deflection $X_r - X_w$
4. Applied voltage to servovalve u_a

From a modelling viewpoint, the three variables ($\ddot{X}_b$, $X_w - X_b$, $X_r - X_w$) may be regarded as system outputs, the control signal ea (equivalent to u_a) is system input, $\dot{X}_r$ and X_r are unmeasured system disturbances.

6.1 **Open-loop state-space model**

For state-space model, the first question for this modelling problem is how to select the state variables. Therefore, the principle for selection is that the set of chosen state variables must be sufficient to control the dynamics of interest system and the numbers of the state variables should be as few as possible to avoid redundancies and should be measured. Theoretically, the total number of state variables to be measured to control the AS model is equal to five.

Displacement sensors (LVDTs) are only able to measure the relative movement of the car body and ground $X_b - X_r$, and the suspension movement of system $X_b - X_w$. In this work, therefore, the practical presentation was considered.

By using the following state-space notations:

$x_1 = \dot{X}_b, \quad x_2 = \dot{X}_w, \quad x_3 = F_{hyd}, \quad x_4 = X_b - X_w, \text{and} \quad x_5 = X_w - X_r$

The system equations may be rearranged to first-order differential equations with differential terms isolated on the left-hand-side.

$$\ddot{X}_b = -\frac{B_{va}}{M_b}\dot{X}_b + \frac{B_{va}}{M_b}\dot{X}_w + \frac{\cos(\alpha \mp \Delta\alpha)}{M_b}F_{hyd} - \frac{1}{M_b}F_{fric} \quad [30]$$

$$\ddot{X}_w = \frac{B_{va}}{M_w}\dot{X}_b - \frac{(B_{va}+b_t)}{M_w}\dot{X}_w - \frac{\cos(\alpha \mp \Delta\alpha)}{M_w}F_{hyd} - \frac{k_t}{M_w}(X_w - X_r) + \frac{b_t}{M_w}\dot{X}_r \quad [31]$$

$$\dot{F}_{hyd} = -\frac{2\beta_{ea}A_c^2}{V}\dot{X}_b + \frac{2\beta_{ea}A_c^2}{V}\dot{X}_w - \frac{2\beta_{ea}}{VR_{ia}}F_{hyd} + \frac{2k_{s\alpha}A_cGP\beta_{ea}}{V}ea \quad [32]$$

$$\dot{X}_b - \dot{X}_w = \dot{X}_b - \dot{X}_w \quad [33]$$

$$\dot{X}_w - \dot{X}_r = \dot{X}_w - \dot{X}_r \quad [34]$$

These equations, with $\Delta\alpha \approx 0.0$, may be written in the state-space form given by:

$$\dot{x} = Ax + Bea + G_d\dot{X}_r \quad [35]$$

Where,

$$x = \text{State vector} = \begin{bmatrix} \dot{X}_b \\ \dot{X}_w \\ F_{hyd} \\ X_b - X_w \\ X_w - X_r \end{bmatrix}$$

$$A = \text{System matrix} = \begin{bmatrix} -\frac{B_{va}}{M_b} & \frac{B_{va}}{M_b} & \frac{\cos\alpha}{M_b} & 0 & 0 \\ \frac{B_{va}}{M_w} & -\frac{(B_{va}+b_t)}{M_w} & -\frac{\cos\alpha}{M_w} & 0 & -\frac{k_t}{M_w} \\ -\frac{2\beta_{ea}A_c^2}{V} & \frac{2\beta_{ea}A_c^2}{V} & -\frac{2\beta_{ea}}{VR_{ia}} & 0 & 0 \\ 1 & -1 & 0 & 0 & 0 \\ 0 & 1 & 0 & 0 & 0 \end{bmatrix}$$

$$B = \text{Input vector} = \begin{bmatrix} 0 \\ 0 \\ \frac{2k_{sa}A_cGP\beta_{ea}}{V} \\ 0 \\ 0 \end{bmatrix}$$

$G = D/A$, gain

$P =$ Forward gain for two-DOF model

$ea =$ Control error signal

$$G_d = \text{Disturbance vector} = \begin{bmatrix} 0 \\ \frac{B_t}{M_w} \\ 0 \\ 0 \\ -1 \end{bmatrix}$$

$\dot{X}_r =$ Disturbance signal, (velocity of road disturbance)

6.2 **Closed-loop system**

When a full-state feedback control law is introduced, as shown in Fig. 8.

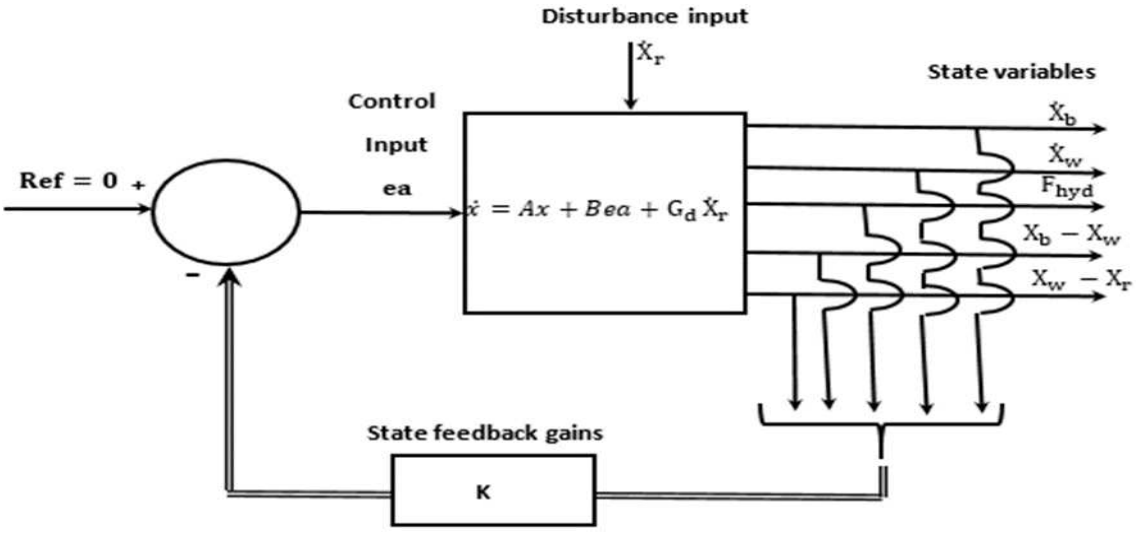

Fig. 8 Full-state feedback control applied to state-space model.

The control error signal becomes a function of all five state variables and feedback gains:

$$\begin{aligned} ea &= -Kx \\ &= -NK_1K_2x \\ &= -N\left(I_1I_2\dot{X}_b + J_1J_2\dot{X}_w + H_1H_2F_{hyd} + F_1F_2\,(X_b - X_w) + L_1L_2\,(X_w - X_r)\right) \end{aligned} \qquad [36]$$

Where

$K = 1$ x 5 State feedback gain vector

$N = A/D$ Gain

$K_1 = 1$ x 5 State feedback gain vector for the controller

$= [\, I_1 \;\; J_1 \;\; H_1 \;\; F_1 \;\; L_1 \,]$

$K_2 = 5$ x 5 Transducer gain matrix

$$K_2 = \begin{bmatrix} I_2 & 0 & 0 & 0 & 0 \\ 0 & J_2 & 0 & 0 & 0 \\ 0 & 0 & H_2 & 0 & 0 \\ 0 & 0 & 0 & F_2 & 0 \\ 0 & 0 & 0 & 0 & L_2 \end{bmatrix}$$

The problem of the active suspension design is how to achieve the gains of the five state variables that allow the system to minimise $\ddot{X}_b$ within the physical constraints ($X_w - X_b$ and $X_r - X_w$) and the limitation of the control input (u_a).

7. Pole-assignment control (PA)

This section presents the design method commonly called the pole-placement or pole-assignment technique. It will be proved that all variables are measurable and available for feedback, if the system is wholly considered stated controllable, accordingly, poles of the closed-loop system are placed at any desired location using state feedback through an appropriate state feedback gain matrix.

In a single-input-single-output control system, a controller (compensator) is designed such that dominant closed-loop poles have a desired damping ratio (ξ) and undamped natural frequency (ω_n), i.e. with acceptable values for maximum overshot and the settling time. Unlike specifying only the dominant closed-loop poles, the PA technique as mentioned by (45) and (2), allows the designer to specify all the closed-loop poles. However, there is a cost associated with employing all the closed-loop poles, because it requires successful measurements of all state variables and must be completely state-controllable.

Considerable of the AS is equivalent to the regulator control system experienced with unmeasured road input disturbances. More precisely, it is desirable to keep all the state variables at zero references in the occurrence of disturbances. With the power of the PA technique, the closed-loop poles can be located at specific locations in the s-plane. In general, the closed-loop poles are specified such that the system dynamic is dominated by an ideal second-order system. This allows the desired damping ratio (ξ) and undamped natural frequency (ω_n) of the dominant poles to be specified.

For a regulator controller type, therefore, the disturbance term should be ignored. Equation [35] became,

$$\dot{x} = Ax + Bu_a \quad [37]$$

Substituting Equation [36] into Equation [37] gives:

$$\dot{x} = (A - BK)x \quad [38]$$

Stability and transient-response characteristics are determined by the eigenvalues of the matrix $(A - BK)$, i.e. regulator poles. If vector K is chosen properly, the matrix $A - BK$ can be made a stable matrix.

To make these control gains suitable for the experimental objective, it is useful to use the form of Equation [36]; the state feedback gain for the controller becomes:

$$K_1 = N^{-1}KK_2 \quad [39]$$

It was found K_1 is,

K_1 = [-0.0035 0.0098 0.21 785.33 2608.34]

Note: For more detail, the design steps can be declared as shown in **APPENDEX.**

8. Comparison between passive suspension and active suspension designed by pole-assignment control realtive to step road excitation

The dynamic performances of the active suspensions designed by pole-assignment control were investigated by simulation using the mathematical model developed previously through using MATLAB m.file to find the K values. Simultaneously, using C++ compiler environment, by developing a code taking into consideration the nonlinear hydraulic actuator, representing the active suspension quarter car mathematical model with the implementation of the nonlinear friction forces that occur at the body bearings. The experiment setup for the validation of pole-assignment control was shown in Fig. 9.

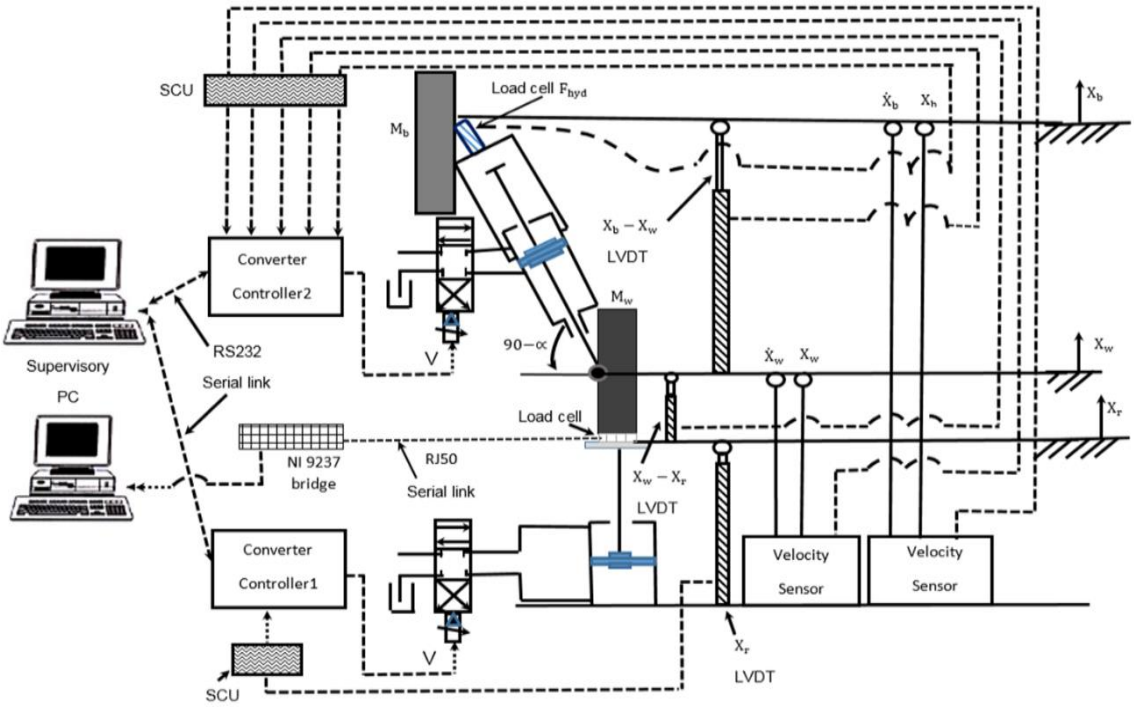

Fig. 9 Experiment setup for the validation of pole-assignment control.

In respect of the force input, therefore, an examination of the values of the relevant variables between the PS and AS systems design in both positive and negative directions is conducted, as introduced in Table III.

Table III: Performance comparisons for passive and PA active suspension control

Concerned variables	Input force Direction	PS	AS (PA)	%Improvement
Acceleration of car body $\ddot{X}_b$ (m/s^2)	+ ve - ve	1.5 2.14	1.43 1.35	5.0 58.5
Suspension displacement $X_w - X_b$(% of max. value) (cm)	+ ve - ve	1.81 3.29	2.43 4.42	34.2 increase 34.2 =
Tyre deflection $X_r - X_w$ (% of max. value) (cm)	+ ve - ve	0.13 0.287	0.133 0.298	- -
Applied voltage to servovalve u_a (max. value) (v)	+ ve - ve	N/A N/A	- 2.52 4.65	- -

It is evident that the AS provides enhanced performance concerning the design objective of this work, i.e. minimising the $\ddot{X}_b$; the AS able to enhancement the ride equality by reducing the vibration level by 58.5% in a negative direction and 5% in a positive direction. However, this is at the cost of increasing the suspension displacement, which increased by 34.2% in both directions, i.e. the body damping was improved by 34.2%. Relatively, the wheel movements in both PS and AS are quite close. However, there is a slight difference in the tyre deflection responses between both systems. Considering the additional energy only consumed for the AS utilises almost the maximum levels of applied voltage u_a.

Figure 10 shows the simulated time responses of the passive and active suspensions designed by PA controller subject to a ramp and step road profile. It is clearly seen that the attenuation of the vibration achieved by the active is greater than the passive system as it has a lower body acceleration identified the control effectiveness achievement.

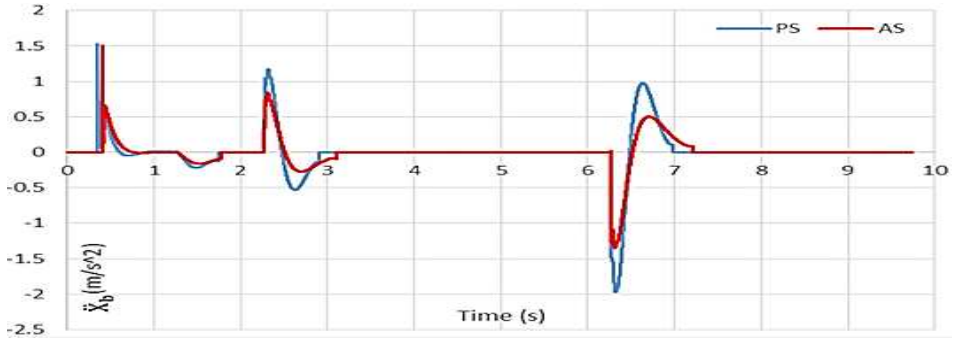

Fig. 10 Comparison of body acceleration between PS and AS

Whereas, the generation hydraulic force for PA controller, in addition to the dominant natural frequency and damping ratio of design, are summarised in Table IV.

Table IV: comparisons of natural frequencies, damping ratios and hydraulic force for passive and active suspension design

Concerned parameters	PS		AS
Dominant natural frequency $\boldsymbol{\omega_n}$ (Hz)	1.4		1.6
Damping ration $\boldsymbol{\xi}$	0.15		0.76
Hydraulic force $\mathbf{F_{hyd}}$ (N)	N/A N/A		+ve 305 -ve 561

It is apparent that the AS takes place at very high damping in comparison to the PS, the real configuration of the PS has a relatively low damping ratio ($\xi = 0.15$); therefore, the effects of the natural frequency of the car body ($\omega_n = 1.4$ Hz) and that of the wheel unit ($\omega_n = 13.6$ Hz) are inevitably dominant. In this work, the design suggestion solution for the AS occurs for $\omega_n = 1.6$ Hz and $\xi = 0.76$. The magnitude response is dramatically reduced around the natural frequency of the car body and its peak shifts slightly to a higher frequency.

In the current study, some of the previous comparisons between the experimental and simulation model results of the PS system demonstrated to show the mathematical modelling validation (1).

Figure 11 shows a comparison between the experimental and simulation system inputs; this figure displayed the desired inputs (X_{rd}), is mixed between the ramp and the step input (∓ 50 mm amplitude), which is passed through a first-order filter to be more convenient with the test rig, and the road input measured X_r. It is evidently seen that the inputs are quite similar in both experiment and simulation, this is vital to make a good paralleling between them, this input is also used for both PS and AS systems.

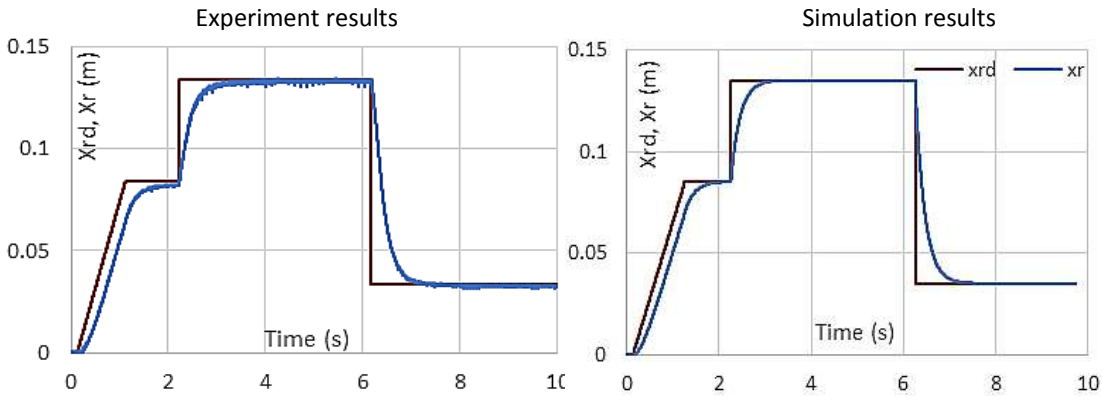

Fig. 11 Comparison of the desired and measured step input X_{rd}, X_r (m) (1).

Figure 12 shows the body velocity responses measured and simulation model results for PS system. It is observed that there is a good agreement between them with a slim difference in values; the velocity model has values higher than the experiment. This is often happening regard to power loss. This consistency is undoubtedly gained from considering friction forces.

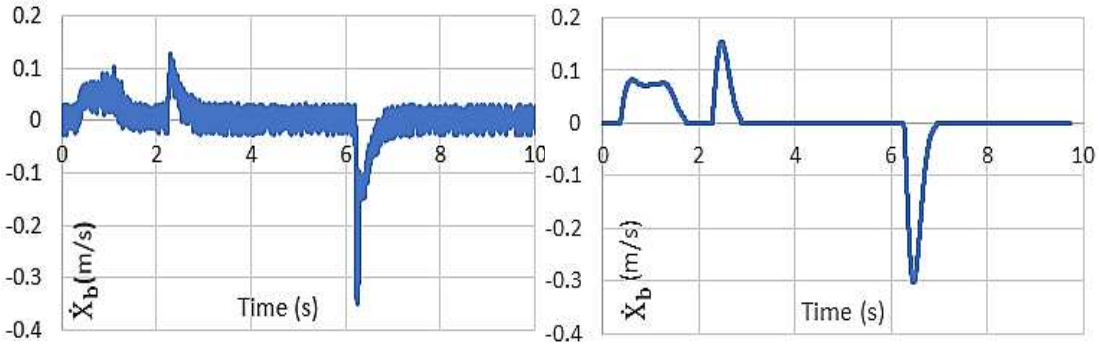

Fig. 12 Body velocity results $\dot{X}_b$ (m/s) for both experimental and simulation (1).

Whereas, Fig. 13 shows the suspension movements $(X_w - X_b)$ for experimental and simulator model results for PS system. It is undoubtedly seen that at the beginning test time, there are high differences between the wheel and body travels according to friction effects, but in general, there is a good agreement between experimental and simulation results. However, the experimental results with extremely noises that might be because of the sensor sensitivity.

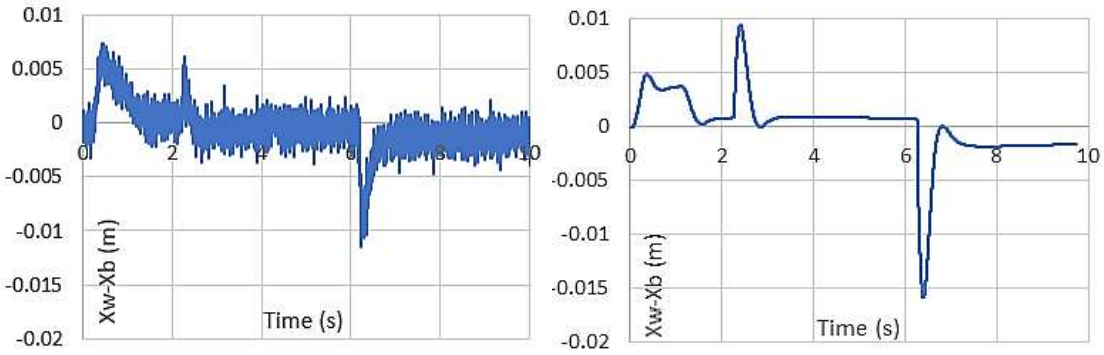

Fig. 13 Comparison of the relative $(X_w - X_b)$ (m) between experimental and simulation results (1).

Correspondingly, to know the extent to which use of the AS enhances the system performance, it is necessary to make a satisfactory comparison between these two systems by using the similar system force inputs.

However, Fig. 14 demonstrates the comparison between the wheel and body movements for PS and AS systems. It is evident that the body travels for AS have a higher delay than PS, i.e. the body damper increases according to control action, accordingly, the body is consumed a considerable time to reach a steady state.

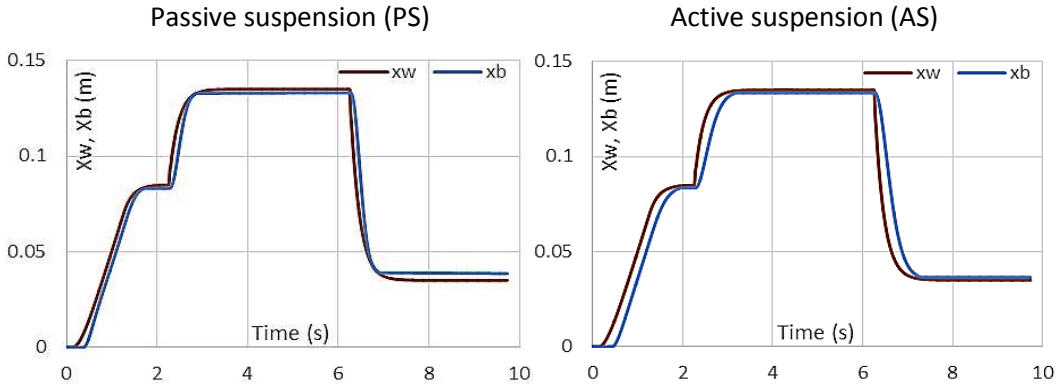

Fig. 14 Comparison of the wheel and body movements.

The suggested PA controller behaviour as a function of time is illustrated in Fig. 15.

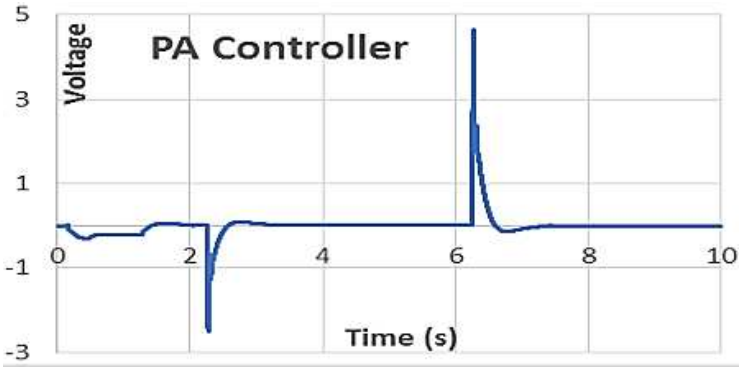

Fig. 15 Suggested PA controller as function of time.

Whereas, the damping of the body velocity for AS is clearly shown in Fig. 16, in comparison with the velocity behaviour for PS, this is, matching with the primary target of control, minimising the body acceleration.

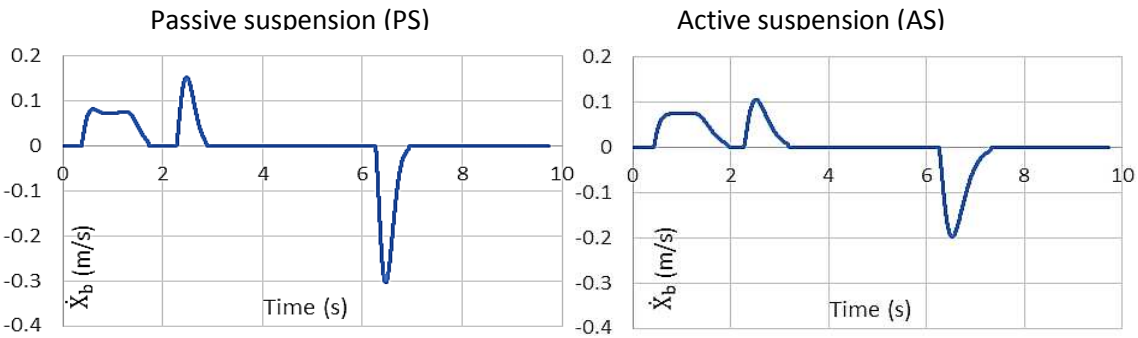

Fig. 16 Comparison between the body velocities for both PS and AS system.

Finally, the suspension movement comparison between the PS and AS demonstrates in Fig. 17, it is evident that the suspension movement is enlarged with AS compared with that for PS that because of the body displacement decreases.

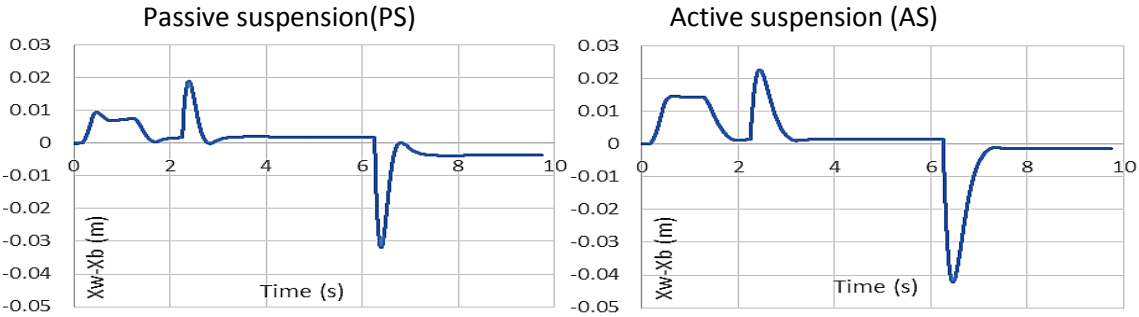

Fig. 17 The suspension movement for PS and AS.

9. Simulation results for passive suspension and active suspension designed by pole-assignment under random road excitation

It was used the existing hydraulic system to generate the random inputs, therefore, the inputs is consisted of the ramp and random inputs.

Three vehicle speeds were tested (50, 100 and 150 km/h) and, due to the random nature of the road profile, the simulation was carried out for each vehicle speed, with a time duration of 10 s. The simulated time responses of the passive and active suspensions

subject to a bump road profile, as described by Equation [6] at different vehicle forward speeds, are given in Fig. 18. It is clear seen that the active decreases the acceleration more efficiently than the passive suspension for all vehicle speeds. However, this is at the cost of increasing the suspension displacement. At higher vehicle forward speeds, the performance of the active suspension is also improved as the suspension travel is reduced compared to that at lower vehicle speeds. These results determine once again that the proposed controller (PA) can improve the ride quality of the driver.

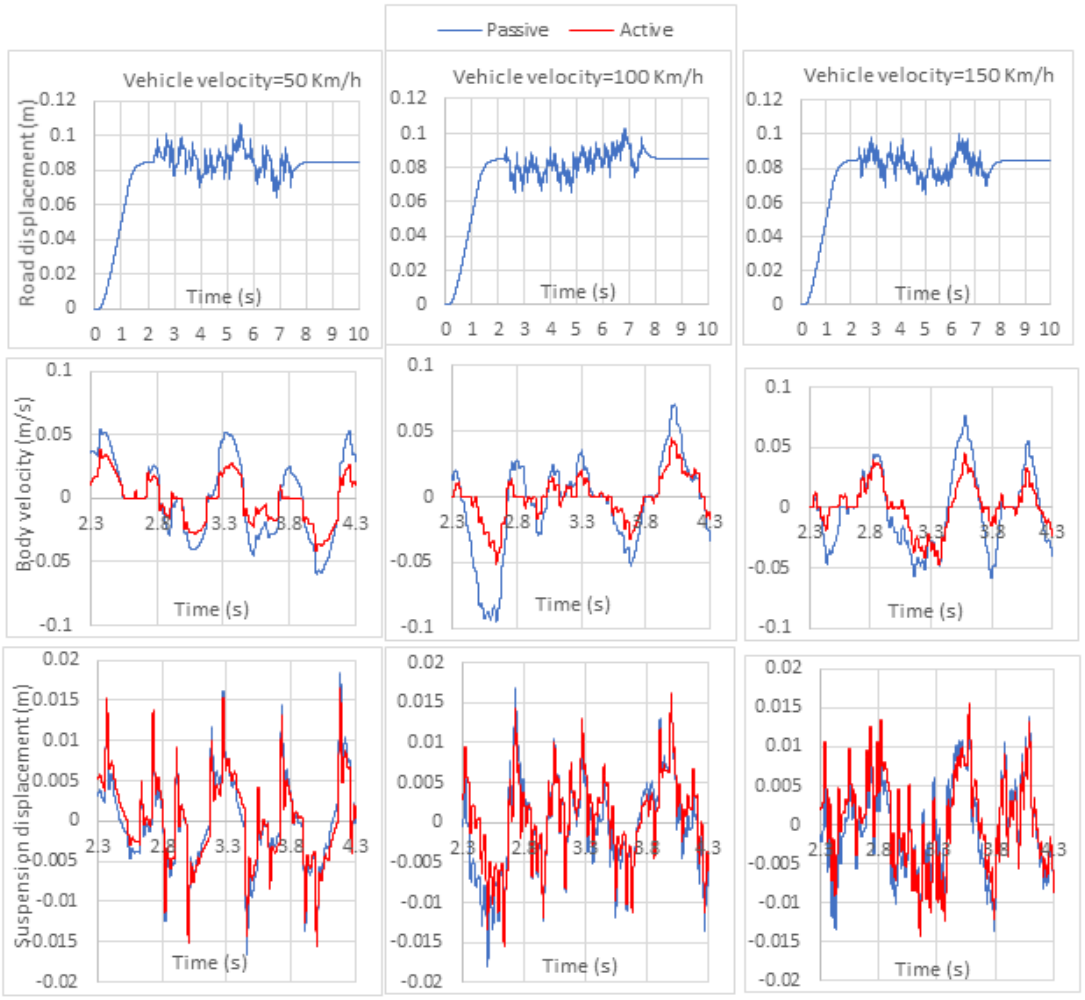

Fig. 18 Simulated time responses of the active and passive under random road excitation and different vehicle speeds.

10.Conclusion

The PA controller has been successfully implemented through servovalve, which leads the nonlinear hydraulic actuator in the active suspension system through a simulation study. Throughout the research, the passive and active suspension system has been developed, and the performance of active suspension system has been proven to perform better than the passive suspension system. For both the PS and AS models, subsequent implementation of the nonlinear friction forces that affect the linear supported body bearings, are entirely accurate and useful. The nonlinear friction model captures most of the friction behaviours that have been observed experimentally, such as stiction region, Stribeck effects, the Coulomb and viscous frictions, which are individually responsible for causing the relatively high differences between the wheel and body travels at the beginning of the test time and the rest behaviours. In addition, the nonlinear hydraulic actuator covered with the dynamic equation of servovalve model is moderately precise and practical. The suggested PA control successfully guided the hydraulic actuator to validate the control strategy. Both simulation and experimental results for the passive suspension system showed consistent agreement between experimental and simulation output, which consequently confirmed the feasibility of the newly approved model that took account of the actual configuration of test rig systems. Whereas, the simulation results for the PS and AS clearly showed the enhancement of system response for both road excitations (ramp and step or random). Although, this study founding an accurate model for ¼-car research test rig that undoubtedly helps to gain accurate modelling and control for active vehicle suspension system, it potentially helps in encouraging researchers to implement a sliding contact design for PS and AS systems with chassis, which directly influences vehicle ride comfort and road handling. For future work, it might be advisable to design LQR or PID controller for AS system instead of the PA

controller, monitoring and employing the contact patch load as feedback control; the current test rig able to measure this force to investigate and enhance system response.

APPENDIX: CONTROL DESIGN STEPS

The design steps can be declared as flowing.

Step l: **Check controllability condition of the system**.

The controllability condition stated that the system must have been completely stating controllable so that all of the eigenvalues of the matrix $(\mathrm{A}-\mathrm{BK})$ can be controlled by state feedback. An analytical proof can be seen from (46), to show that a necessary and sufficient condition for arbitrary pole placement to be the system completely states controllable. A controllability matrix $\mathrm{M_c}$ is constructed from the system matrix A and the input vector B as follows:

$$\mathrm{M_c} = [\mathrm{B}\ \ \mathrm{AB}\ \ \mathrm{A^2B}\ \ \mathrm{A^3B}\ \ \mathrm{A^4B}] \qquad [40]$$

If the matrix $\mathrm{M_c}$ having order $\mathrm{n} * \mathrm{n}$ is said to have rank n if its determinant is non-zero, that is, i.e. the condition for the controllability can be written in a mathematical form as:

$$\text{If } |\mathrm{M_c}| \neq 0 \quad \text{ then rank } [\mathrm{M_c}] = \mathrm{n} \qquad [41]$$

If rank $[\mathrm{M_c}]$ is equal to n (necessary condition). Therefore, the matrix $(\mathrm{A}-\mathrm{BK})$ can be made an asymptotically stable matrix if matrix **K** is selected correctly. It was found that $\mathrm{n} = 5 \text{ and } |\mathrm{M_c}| = -8.5978e23$.

Step 2: **Determine the coefficients of the characteristic polynomial.**

If the system ultimately states controllable, condition [41], then all eigenvalues of matrix **A** can be arbitrarily placed.

From the characteristic polynomial for the matrix **A**:

$$|\mathrm{sI} - \mathrm{A}| = a_0 + a_1\, s + a_2 s^2 + a_3 \mathrm{s}^3 + a_4 \mathrm{s}^4 + a_5 s^5 \quad [42]$$

Determine the values of a_0, a_1, a_2, a_3, a_4 and a_5, it was found that,

$|\mathrm{sI} - \mathrm{A}| = 10817345.3\ s + 351225.5\, s^2 + 20608.27\, \mathrm{s}^3 + 133.38\, \mathrm{s}^4 + s^5$

Step 3: **Determine the transformation matrix T that transforms the system state equation into the control canonical form.**

The matrix T is given by:

$$\mathrm{T} = \mathrm{M_c W_c} \quad [43]$$

Where $\mathrm{M_c}$ = controllability matrix and $\mathrm{W_c}$ is given by:

$$\mathrm{W}_c = \begin{bmatrix} a_1 & a_2 & a_3 & a_4 & 1 \\ a_2 & a_3 & a_4 & 1 & 0 \\ a_3 & a_4 & 1 & 0 & 0 \\ a_4 & 1 & 0 & 0 & 0 \\ 1 & 0 & 0 & 0 & 0 \end{bmatrix} \quad [44]$$

Step 4: **Specify a set of the desired eigenvalues.**

The closed-loop pole locations must be chosen in such a way that the system outputs behave similarly to a standard second-order system. The closed-loop pole locations could be obtained as follows:-

$$\mu = -\sigma \pm \omega_d j \quad [45]$$

Where,

$$\sigma = \xi\omega_n \ \text{ And } \ \omega_d = \omega_n\sqrt{1 - \xi\text{^}2} \quad [46]$$

$\xi = 0.76\ and\ \omega_n = 1.56$ Hz, are selected depending on the values of settling time and maximum overshoot were accepted.

Therefore, the desired closed-loop poles for the active suspension are:

$$\mu_1 = -\sigma + \omega_d j, \qquad \mu_1 = -7.45 + 6.37j$$
$$\mu_2 = -\sigma - \omega_d j, \qquad \mu_2 = -7.45 - 6.37j$$
$$\mu_3 = -10\sigma, \qquad \mu_3 = -74.5 \qquad [47]$$
$$\mu_4 = -10\sigma, \qquad \mu_3 = -74.5$$
$$\mu_5 = -10\sigma, \qquad \mu_3 = -74.5$$

The dominant closed-loop poles of the system designs used the three output variables are plotted by Pole-Zero closed system map in Fig. 19.

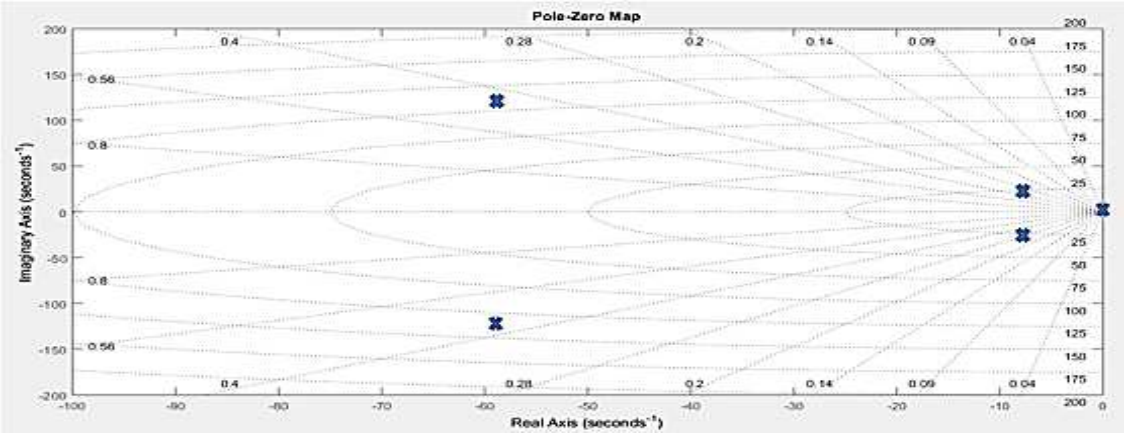

Fig. 19 Pole-Zero closed system map for (X_b- X_w), (X_w- X_r) and F_{hyd} feedbacks

Whereas, the relationship between ω_n, ξ and the locations of the suggested five closed-loop poles in the s-plane relative to the ideal second-order response are elucidated in Fig. 20. The μ_1 and μ_2 terms are a pair of dominant closed-loop poles, the remaining three closed-loop poles are located far to the left to make the system faster, while the damping of the system will be mainly caused by the dominance of the closed-loop poles.

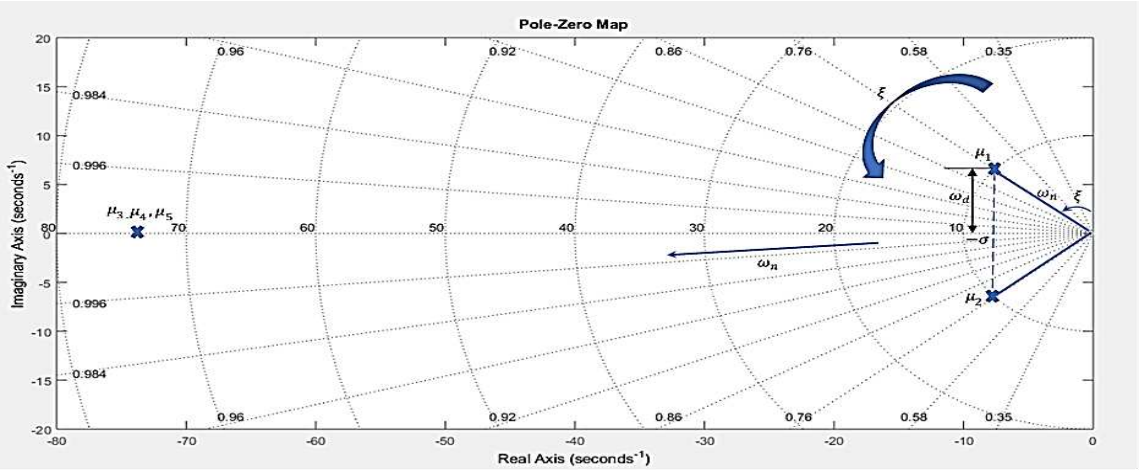

Fig. 20 Location of the five suggested closed-loop poles for PA controller in Pole-Zero map

Step 5: **Determine the desired characteristic equation.**

From the desired characteristic polynomial:

$(s-\mu_1)(s-\mu_2)(s-\mu_3)(s-\mu_4)(s-\mu_5) = \alpha_0 + \alpha_1\, s + \alpha_2\, s^2 + \alpha_3\, s^3 + \alpha_4\, s^4 + \alpha_5 s^5$ [48]

Determine the values of $\alpha_0, \alpha_1, \alpha_2, \alpha_3, \alpha_4$ and α_5, it was found that:

$= 3.97e7 + 7.76e6\, s + 6.83e5\, s^2 + 2.01e4\, s^3 + 2.38e2\, s^4 + s^5$

Step 6: **Determine state feedback vector K.**

Therefore, by using [39] the characteristic equation for this system is:

$$|\mathrm{sI} - \mathrm{A} + \mathrm{BK}| = |\mathrm{T}^{-1}\,(\mathrm{sI} - \mathrm{A} + \mathrm{BK})\mathrm{T}| = |\mathrm{sI} - \mathrm{T}^{-1}\mathrm{AT} + \mathrm{T}^{-1}\mathrm{BKT}| = 0 \qquad [49]$$

$$|\mathrm{sI} - \mathrm{T}^{-1}\mathrm{AT} + \mathrm{T}^{-1}\mathrm{BKT}| = (a_0 + \delta_0) + (a_1 + \delta_1)s + (a_2 + \delta_2)s^2 + (a_3 + \delta_3)\mathrm{s}^3 + (a_4 + \delta_4)\mathrm{s}^4 + s^5 \qquad [50]$$

This is the characteristic equation for a system with state feedback. Therefore, it must be equal to Equation [50], the desired characteristic equation. By equating the coefficients of like powers of s, we obtain:

$$\delta_0 = \alpha_0 - a_0\,, \delta_1 = \alpha_1 - a_1, \delta_2 = \alpha_2 - a_2\,, \delta_3 = \alpha_3 - a_3\,, \delta_4 = \alpha_4 - a_4 \qquad [51]$$

Let us write,

$$KT = [\delta_0 \quad \delta_1 \quad \delta_2 \quad \delta_3 \quad \delta_4] \qquad [52]$$

The required state feedback gain can be determined by the equation:

$$K = [\delta_0 \quad \delta_1 \quad \delta_2 \quad \delta_3 \quad \delta_4]T^{-1} \qquad [53]$$

It was found K,

$$K = [-2.27 \quad 6.45 \quad 0.0014 \quad 19.8 \quad 230.7]$$

To make these control gains suitable for the experimental objective, it is useful to use the form of Equation [68]; the state feedback gain for the controller becomes:

$$K_1 = N^{-1}KK_2 \qquad [54]$$

It was found K_1,

$K_1 =$ [-0.0035 0.0098 0.21 785.33 2608.34]

References:

1. Alzughaibi A, Xue Y, Grosvenor R. A new insight into modelling passive suspension real test rig system with consideration of nonlinear friction forces. Proceedings of the Institution of Mechanical Engineers, Part D: Journal of Automobile Engineering. 2018;0(0):0954407018764942.
2. Dorf RC, Bishop RH. Modern control systems: Pearson; 2011.
3. Goodwin GC, Graebe SF, Salgado ME. Control system design2001.
4. Brogan WL. Modern control theory. New Jersy: : Prentice Hall; 1991. 317 p.
5. Yang M, Yang Y, Zhang D, Jia X, editors. PID control for a height adjustable wheel-direct-drive system via time-varying samplings. Control Conference (CCC), 2016 35th Chinese; 2016: IEEE.
6. Kumar MS. Development of active suspension system for automobiles using PID controller. 2008.
7. Gao H, Lam J, Wang C. Multi-objective control of vehicle active suspension systems via load-dependent controllers. Journal of Sound and Vibration. 2006;290(3):654-75.
8. Fei J, Xin M. Robust adaptive sliding mode controller for semi-active vehicle suspension system. International Journal of Innovative Computing, Information and Control. 2012;8(1):691-700.
9. Ramli H, Meon M, Mohamed T, Isa A, Mohamed Z. A Fuzzy-Active Force Control Architecture Based in Characterizing Nonlinear Systems' Behavior. Procedia Engineering. 2012;41:1389-97.
10. Fax JA, Murray RM. Information flow and cooperative control of vehicle formations. IEEE transactions on automatic control. 2004;49(9):1465-76.

11. Li Z, Duan Z, Chen G, Huang L. Consensus of multiagent systems and synchronization of complex networks: A unified viewpoint. IEEE Transactions on Circuits and Systems I: Regular Papers. 2010;57(1):213-24.
12. Zhang H, Lewis FL, Das A. Optimal design for synchronization of cooperative systems: state feedback, observer and output feedback. IEEE Transactions on Automatic Control. 2011;56(8):1948-52.
13. Li Z, Ren W, Liu X, Xie L. Distributed consensus of linear multi-agent systems with adaptive dynamic protocols. Automatica. 2013;49(7):1986-95.
14. Li Z, Wen G, Duan Z, Ren W. Designing fully distributed consensus protocols for linear multi-agent systems with directed graphs. IEEE Transactions on Automatic Control. 2015;60(4):1152-7.
15. Herman I, Sebek M, editors. Optimal distributed control with application to asymmetric vehicle platoons. Decision and Control (CDC), 2016 IEEE 55th Conference on; 2016: IEEE.
16. Ma X, Wong PK, Zhao J. Practical multi-objective control for automotive semi-active suspension system with nonlinear hydraulic adjustable damper. Mechanical Systems and Signal Processing. 2019;117:667-88.
17. Zhao J, Wong PK, Ma X, Xie Z. Chassis integrated control for active suspension, active front steering and direct yaw moment systems using hierarchical strategy. Vehicle System Dynamics. 2017;55(1):72-103.
18. Zhao J, Wong P, Ma X, Xie Z. Design and analysis of an integrated SMC-TPWP strategy for a semi-active air suspension with stepper motor-driven GFASA. Proc Inst Mech Eng Part I J Syst Control Eng. 2018.
19. Ibrahim R. Friction-induced vibration, chatter, squeal, and chaos—part II: dynamics and modeling. Appl Mech Rev. 1994;47(7):227-53.
20. Ibrahim R. Friction-induced vibration, chatter, squeal, and chaos, Part I: Mechanics of contact and friction. Applied Mechanics Reviews. 1994;47(7):209-26.
21. Simpson T, Ibrahim R. Nonlinear friction-induced vibration in water-lubricated bearings. Modal Analysis. 1996;2(1):87-113.
22. Berger E. Friction modeling for dynamic system simulation. Applied Mechanics Reviews. 2002;55(6):535-77.
23. Rabinowicz E. The nature of the static and kinetic coefficients of friction. Journal of applied physics. 1951;22(11):1373-9.
24. Brockley C, Cameron R, Potter A. Friction-induced vibration. ASME J Lubr Technol. 1967;89(2):101-8.
25. Brockley C, Davis H. The time-dependence of static friction. Journal of Lubrication Technology. 1968;90(1):35-41.
26. Plint A, Plint M. A new technique for the investigation of stick-slip. Tribology international. 1985;18(4):247-9.
27. Ibrahim R, Zielke S, Popp K. Characterization of interfacial forces in metal-to-metal contact under harmonic excitation. Journal of sound and vibration. 1999;220(2):365-77.

28. Pilipchuk V, Olejnik P, Awrejcewicz J. Transient friction-induced vibrations in a 2-DOF model of brakes. Journal of Sound and Vibration. 2015;344(Supplement C):297-312.
29. Wielitzka M, Dagen M, Ortmaier T, editors. State and maximum friction coefficient estimation in vehicle dynamics using UKF. American Control Conference (ACC), 2017; 2017: IEEE.
30. Agostinacchio M, Ciampa D, Olita S. The vibrations induced by surface irregularities in road pavements–a Matlab® approach. European Transport Research Review. 2014;6(3):267-75.
31. Odrigo A, El-Gindy M, Pettersson P, Nedělková Z, Lindroth P, Öijer F. Design and development of a road profile generator. International Journal of Vehicle Systems Modelling and Testing. 2016;11(3):217-33.
32. Tyan F, Hong Y-F, Tu S-H, Jeng WS. Generation of random road profiles. Journal of Advanced Engineering. 2009;4(2):1373-8.
33. Standardization IOf. Mechanical Vibration--Road Surface Profiles--Reporting of Measured Data. ISO 8608:1995, ISO/TC108/SC2, Geneve: International Organization for Standardization; 1995.
34. Alfadhli A, Darling J, Hillis AJ. The control of an active seat with vehicle suspension preview information. Journal of Vibration and Control. 2018;24(8):1412-26.
35. FitzSimons PM, Palazzolo JJ. Part I: Modeling of a One-Degree-of-Freedom Active Hydraulic Mount. Journal of Dynamic Systems, Measurement, and Control. 1996;118(3):439-42.
36. Merritt HE. Hydraulic control systems: John Wiley & Sons; 1967. p. 316-8.
37. Guo Q, Yu T, Jiang D. High-gain observer-based output feedback control of single-rod electro-hydraulic actuator. IET Control Theory & Applications. 2015;9(16):2395-404.
38. Fu S, Lu S, Kai G. Characteristics and control technology research of three-stage electro-hydraulic servovalve. J Appl Sci Eng Innov. 2015;2(2).
39. Maneetham D, Afzulpurkar N. Modeling, simulation and control of high speed nonlinear hydraulic servo system. Journal of Automation Mobile Robotics and Intelligent Systems. 2010;4:94-103.
40. Alleyne A, Hedrick JK. Nonlinear adaptive control of active suspensions. IEEE transactions on control systems technology. 1995;3(1):94-101.
41. Watton J. Modelling, monitoring and diagnostic techniques for fluid power systems: Springer Science & Business Media; 2007.
42. Eryilmaz B, Wilson BH, editors. Modeling the internal leakage of hydraulic servovalves. International Mechanical Engineering Congress and Exposition, ASME; 2000.
43. Kalyoncu M, Haydim M. Mathematical modelling and fuzzy logic based position control of an electrohydraulic servosystem with internal leakage. Mechatronics. 2009;19(6):847-58.
44. Karpenko M, Sepehri N. Fault-tolerant control of a servohydraulic positioning system with crossport leakage. IEEE Transactions on Control Systems Technology. 2005;13(1):155-61.
45. Katsuhiko O. Modern control engineering. 2010.
46. Ogata K. Modern control engineering. 2010.